Characterization of Parathyroid Hormone/Receptor Interactions: Structure of the First Extracellular Loop†

Andrea Piserchio,‡ Alessandro Bisello,|| Michael Rosenblatt,|| Michael Chorev,|| and Dale F. Mierke*,‡,§

Department of Chemistry, Brown University, Providence, Rhode Island 02912, Division of Bone & Mineral Metabolism, Charles A. Dana and Thorndike Laboratories, Department of Medicine, Beth Israel Deaconess Medical Center, Boston, Massachusetts 02215, Department of Molecular Pharmacology, Physiology, & Biotechnology, Division of Biology and Medicine, Brown University, Providence, Rhode Island 02912

Received February 1, 2000

ABSTRACT: The structural features of the first extracellular loop (ECL1) of the parathyroid hormone receptor (PTH1R) in the presence of dodecylphosphocholine micelles have been determined using high-resolution NMR techniques. The structure of the receptor fragment, PTH1R(241−285), includes three α-helices for residues 241−244, 256−264, and 275−284. The first and third correspond to the end and the beginning of transmembrane helices 2 and 3, respectively. Centrally located in the second helix is L^{261}, found to cross-link to Lys^{27} of parathyroid hormone, PTH(1−34) [Greenberg, Z., Bisello, A., Mierke, D. F., Rosenblatt, M., and Chorev, M. (2000) *Biochemistry 39*, 8142−8152]. On the basis of nitroxide radical-induced relaxation studies, the central helix is found to associate with the surface of the membrane mimetic. These data, in conjunction with previous results indicating a preference of PTH for the lipid surface, suggest a membrane-associated pathway for the initial recognition and binding of PTH to its G-protein-coupled receptor. Using the structural features of ECL1 as determined here, along with the structure of the PTH(1−34), the intermolecular interactions consistent with the contact point between L^{261}(receptor)−Lys^{27}(ligand) are identified.

The parathyroid hormone receptor (PTH1R)[1] is a transmembrane receptor belonging to a subfamily of G-protein-coupled receptors that includes the calcitonin-like receptors, glucagon, secretin, and latrotoxin receptors (*1*−*3*). The receptors are characterized by long extracellular N-termini (∼150 residues) with multiple potential glycosylation sites, a highly conserved pattern of six cysteines in the extracellular N-terminus, and a putative disulfide bond linking the first two extracellular loops (ECLs).

PTH1R is activated by both parathyroid hormone (PTH) and parathyroid hormone-related protein (PTHrP). PTH plays a central role in calcium homeostasis and regulation of bone remodeling and therefore is an important target for the development of a therapy for osteoporosis (*4*−*9*). PTHrP displays a pharmacological profile similar to that of PTH and is associated with skeletal development and humoral hypercalcemia of malignancy (*10*−*15*). An understanding of the molecular mechanism by which these hormones interact with and activate PTH1R would be an important step toward the development of novel drugs for treatment of hypoparathyroidism, hypercalcemia, and osteoporosis.

Unfortunately, structural data of PTH1R are limited to theoretical models, as experimental techniques (NMR or X-ray analysis) are not currently generally applicable to transmembrane (TM) receptors. These models (*16*, *17*) are based on the experimental results obtained for the ubiquitous rhodopsin and bacteriorhodopsin (*18*−*21*). Results from site-directed mutagenesis studies (*22*−*25*) and incorporation of zinc binding domains (*26*) validate the use of these unrelated receptors as templates for the arrangement and topological orientation of the transmembrane helices of PTH1R (*16*). Importantly, the template models do not provide structural information of the ectopic and cytoplasmic portions of the receptor. The extracellular domain of the receptor is vital for ligand recognition and binding (*27*−*29*), while the intracellular portion is responsible for the coupling to G-proteins and adaptor molecules (e.g., β-arrestins) (*30*−*32*).

To address this issue, we have undertaken the structural characterization of the loops and selected regions of the termini of PTH1R (*33*−*36*). This approach was recently applied to rhodopsin (*37*, *38*). In the design of the receptor fragments, it is important to incorporate a sufficient number

† This work was supported in part by NIH Grants R29-GM54089 (D.F.M.) and RO1-DK47940 (M.R.).

* To whom correspondence should be addressed at Department of Molecular Pharmacology, Physiology, & Biotechnology, Division of Biology and Medicine, Box G-B4, Brown University, Providence, RI 02912. Voice: (401) 863-2139. Fax: (401) 863-1595. E-mail: Dale_Mierke@Brown.edu.

‡ Department of Chemistry, Brown University.

|| Beth Israel Deaconess Medical Center.

§ Department of Molecular Pharmacology, Physiology, & Biotechnology, Brown University.

[1] Abbreviations: DG, distance geometry; DQF-COSY, double quantum filtered correlation spectroscopy; DPC, dodecylphosphocholine; ECL1−3, extracellular loops 1−3; G-protein, guanine nucleotide-binding regulatory protein; GPCR, G-protein coupled receptor; MD, molecular dynamics; ICL1−3, intracellular loops 1−3; NOE, nuclear Overhauser enhancements; NOESY, nuclear Overhauser enhancement spectroscopy; PTH, human parathyroid hormone; PTH1R, parathyroid hormone receptor 1; PTHrP, parathyroid hormone-related protein; PDB, Brookhaven Protein Databank; RMSD, root-mean-square deviation; TOCSY, total-correlation spectroscopy; TM, transmembrane.

10.1021/bi000196f CCC: $19.00
Published on Web 06/16/2000

of amino acids of the adjacent TM helices to act as anchors, tethering the loop or termini to the lipid environment and providing the naturally occurring topological orientation. The resulting structural findings can then be incorporated into the model of the full receptor, providing the experimentally based conformational preferences of the loops and termini together with the arrangement of the TM helices (*16*). One important result of these investigations is the identification of the exact location of each end of the TM helix. The structural features of the receptor fragments, coupled with the findings from photoaffinity cross-linking data (*39*−*43*), have provided unique insight into the details of ligand−receptor interactions.

Here, we examine the conformation of the first extracellular loop (ECL1) of PTH1R, PTH1R(241−285),[2] by ^{1}H NMR in the presence of dodecylphosphocholine (DPC) micelles. The structural features are obtained by applying the experimental data in extensive distance geometry and molecular dynamics simulations using a two-phase, water/decane simulation cell (*36*).

EXPERIMENTAL PROCEDURES

Materials. Boc-protected amino acids, *N*-hydroxybenzotriazole (HOBt), *N*,*N*′-dicyclohexylcarbodiimide, and *p*-methylbenzydrylamine resin were purchased from Applied Biosystems (Foster City, CA). B&J brand dichloromethane, acetonitrile, methanol, and *N*-methylpyrrolidone (NMP) were obtained from Baxter (McGraw Park, IL). Trifluoroacetic acid was from Aldrich.

Peptide Synthesis. The synthesis of ECL1 (Ac-DAVLYSGATLDEAERLTEEELRAIAQAPPPPATAAAGYAGBRVAV-NH_2), where B is norleucine replacing C281 of the wild-type receptor, was carried out by solid-phase methods on *p*-methylbenzydrylamine resin using standard Boc/HOBt/NMP chemistry and liquid hydrogen fluoride (HF) cleavage as described previously (*44*). Following HF cleavage, ECL1 was purified by HPLC as described (*44*) using a linear gradient from 15 to 45% B in A in 90 min, where eluant A is 0.1% TFA in water, and eluant B is 0.1% TFA in acetonitrile. Purity and structural integrity of ECL1 were confirmed by analytical HPLC, amino acid analysis, and electron spray ionization (ESI)−mass spectrometry (MS).

NMR Spectroscopy. The peptide was dissolved in water (2 mM, 10% D_2O, pH 4.5 uncorrected) in the presence of 150 mM dodecylphosphocholine-d_{38} (Cambridge Isotopes Laboratory). All the NMR spectra were recorded on a Bruker Avance 600 and a home-built 750-MHz spectrometer at 298 and 323 K. Tetramethylsilane was used as reference (0.0 ppm). The spectra were analyzed using XwinNmr (Bruker), Felix (Biosym/MSI, San Diego), nmrPipe (*45*), and Sparky (UCSF).

Total correlation spectroscopy (TOCSY) and double quantum filtered correlation spectroscopy (DQF-COSY) experiments were used to identify the amino acid spin systems. An MLEV-17 sequence, with a spin-lock field of 10 000 Hz, was employed for the TOCSY mixing times (typically 50 ms). Nuclear Overhauser enhancement spectroscopy (NOESY) experiments with a mixing time between 70 and 150 ms allowed for the sequential assignment and determination of interproton distances. Water suppression was obtained using the WATERGATE sequence or with gradient selection of coherence pathway (*46*). Secondary shifts for Hα protons were calculated by subtracting the standard chemical shift values for random peptides from the measured ones and averaged over five residues (*47*).

Topological Orientation. The topological orientation of the peptide relative to the lipid surface was determined by addition of 5- and 12-doxylstearic acid, following published procedures (*35*, *36*, *48*). The long, lipophilic chain readily inserts into the micelles and places the radical at different depths from the surface (just under the zwitterionic interface for 5-doxylstearic acid, approximately in the center of the micelle for 12-doxylstearic acid) (*48*, *49*). 1D and TOCSY experiments (mixing time 35 ms) were recorded under identical conditions before and after the addition of the doxylstearic acid. The intensities of cross-peaks involving both backbone (H^N-H^α) and side chain protons ($H^\alpha-H^\beta$, $H^\gamma-H^\delta$) were compared.

Distance Geometry. Cross-peak volumes from the NOESY spectra were integrated and converted into distance restraints using the two-spin approximation (with resolved cross-peaks between methylene protons used as reference). A matrix of experimental upper and lower bounds was obtained adding and subtracting 10% to each NOE-derived distance. Pseudoatom corrections were then applied to the upper bounds of all methyl groups and all unresolved methylene protons (*50*). A distance matrix containing upper and lower bounds was built by merging matrixes derived from the NOEs and molecular constitution of the molecule (*51*). Using random metrization (*52*), 100 structures were generated. The structures were optimized initially in four dimensions and then in three-dimensional space via conjugate gradients and distance driven dynamics (*53*, *54*). Structures with NOE violations greater than 0.2 Å or having high energy due to structural distortion were manually discarded. Following this procedure, 98 structures fulfilling the interproton experimental distances and the holomonic constraints were obtained. All the calculations were performed on an SGI O2 station using home-written programs.

Molecular Dynamics. One of the structures with low violations obtained from distance geometry (DG) was energy-minimized with conjugate gradients using the AMBER force field (ignoring charges) using DISCOVER (Molecular Simulations, Inc.). The resulting model was soaked in a periodic, two-phase cubic box of dimension 840 nm^3 containing 700 decane molecules and 7700 molecules of water. InsightII was used to interactively orient the peptide in the solvation cell. Molecular dynamics (MD) simulations were performed using GROMACS, version 1.6 (*55*). All atoms belonging to the peptide and the water were treated explicitly in a GROMOS-87 force field including Lennard Jones (within 8 Å), Coulomb (within 10 Å), and standard bonded interactions (bond stretching, bond angles vibration, and improper dihedrals). The parameters for decane appears elsewhere (*56*). The CH_2 and CH_3 groups of decane were treated as united atoms, the Ryckaert−Bellemans potential was applied, and a minimum distance of 0.23 nm between water and decane molecules was allowed (*56*).

Initially, the system was energy-minimized for 100 steps, and the solvent−peptide interactions optimized by 10 ps of

[2] For clarity, the one letter code will be used for the residues of the receptor, and the three letter code will be used for the residues of the ligand.

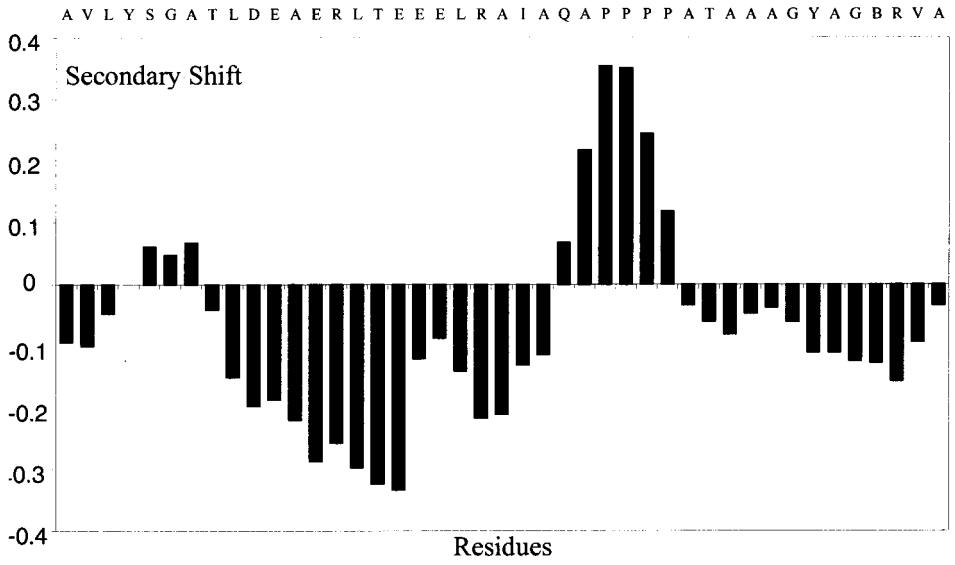

FIGURE 1: Secondary shifts of α-protons of PTH1R(241−285) in aqueous solution (2.0 mM, pH 4.5) in the presence of DPC (150 mM) micelles.

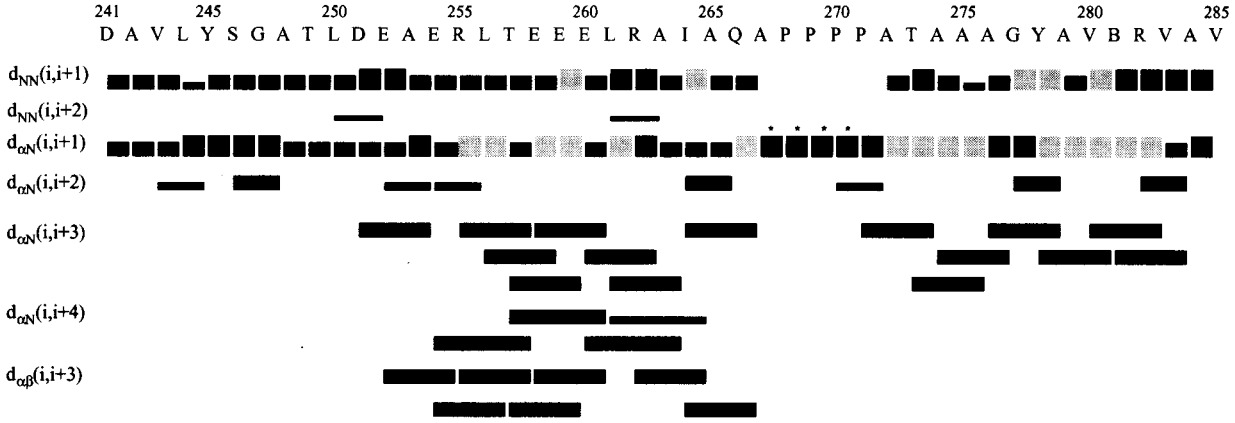

FIGURE 2: Relevant NOEs detected from NOESY spectra between 293 and 323 K, utilized in the structure refinement calculation. NOEs are divided into three categories according to their intensities (strong, medium, and weak). A shaded bar indicates a cross-peak partially overlapped, and the symbol (*) indicates an (α → δ) interaction.

MD simulation with the peptide restrained to its starting conformation (force constant of 1000 kJ mol^{-1} nm^{-1}). The experimental distance constraints were then introduced (force constant of 10 000 kJ mol^{-1} nm^{-1}) and 400 ps of MD carried out at 300 K with a temperature bath coupling of 0.02 ps. The equations of motions were integrated every 2 fs, neighbors lists for long-range interactions were updated every 10 steps, and the resulting trajectories were sampled every 0.5 ps. All MD calculations were performed on a SGI Origin 2000 computer.

RESULTS

According to homology modeling (*16*), PTH1R(241−285) should include the entire first ECL and five or six hydrophobic residues belonging to TM 2 and 3 at the N- and C-termini, respectively. Our design principle calls for these residues to insert into the hydrophobic environment provided by the lipid micelle and serve as anchors for ECL1. In fact, the lipid micelles are required to prevent the aggregation and precipitation of these receptor fragments (*35*, *57*). DPC micelles afford a zwitterionic lipid environment, which because of its small size, tumbles and reorients quickly in solution and therefore is amenable to high-resolution NMR techniques (*36*). Comparisons of structural results obtained with micelles and bilayers have indicated only minor differences (*58*).

NMR Results. The Hα secondary shifts (Figure 1) suggest the presence of at least two helical portions involving approximately $D^{251}-A^{265}$ and $T^{273}-A^{284}$. In particular, the fragment $L^{253}-T^{257}$ exhibits strongly negative secondary shifts (*47*). The positive values observed along the sequence $A^{267}-P-P-P-P-A^{272}$ are consistent with an extended conformation. Finally, the slightly negative values observed for the first few residues of the N-terminus, $D^{241}-A^{248}$, may suggest the presence of a third, nascent helix.

There are many NOEs, shown in Figure 2, of the type α(i)−N(i + 3), α(i)−N(i + 4), and α(i)−β(i + 3) throughout $D^{251}-Q^{266}$ and $A^{272}-A^{284}$ indicative of α-helices. Interestingly, some α(i)−N(i + 2) interactions, usually indicating 3^{10} helices or β-turn-like conformations, were observed at the extremes of the two helical regions. Such NOEs were also present in the N-terminus, $D^{241}-A^{248}$. The observation of all of the possible NH(i)−NH(i + 1) NOEs between resolved protons, illustrated in Figure 3, suggests that the

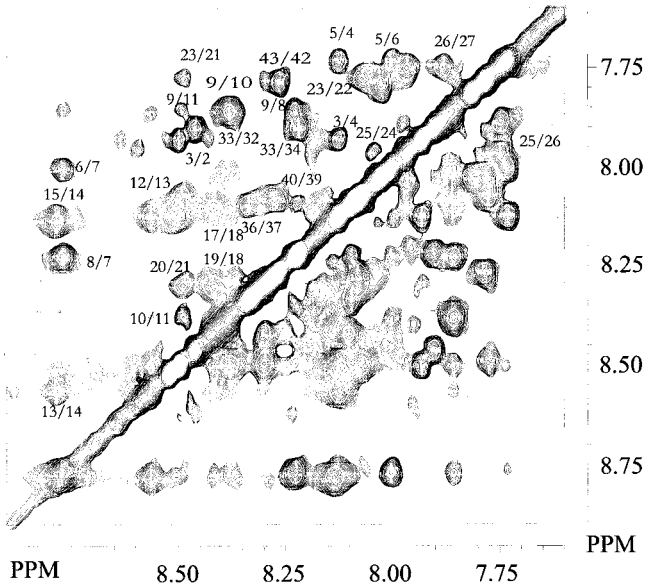

FIGURE 3: Amide region of a NOESY spectrum (318 K, mixing time of 150 ms) in aqueous solution (2.0 mM, pH 4.5) in the presence of DPC (150 mM) micelles. Some of the sequential connectivities are indicated.

peptide is, in general, well-structured (e.g., such NOEs are not expected for random-coil) (*50*).

DG Calculations. The resulting structures from the DG calculations exhibit helical segments encompassing L^{256}–A^{267} and A^{276}–A^{284} (shown in Figure 4). In these two regions, all of the dihedral angle order parameters (*59*) for ϕ and ψ indicate high convergence of the structures except for the angles I^{264} ψ, A^{265} ϕ, and $A^{267}\phi$. Clustering and visual analysis of the structures revealed two families of conformations in this region: one with a well-defined α-helix, and the second containing a less-ordered helical turn ending with a 3^{10} helix-like hydrogen bond between the carbonyl of residue I^{264} and the amide proton of residue A^{267}. Similar combinations of $i \rightarrow i + 3$ and $i \rightarrow i + 4$ turns were also detected for A^{253}–L^{256}. High dihedral angle order parameters are also observed for the four consecutive proline residues between position 268 and 271, all characterized by an extended conformation except for P^{271}, which has negative values for both dihedral angles. The lack of structure in A^{272}–A^{275}, in particular around residue A^{275}, makes the determination of the relative orientation of the central and C-terminal helices impossible. Therefore, the distance between the termini is not well-defined, with values ranging from 18 to 50 Å.

Topological Orientation. Upon addition of 12-doxylstearic acid to the peptide/micelle solution, no changes were detected in the TOCSY spectra. In contrast, almost all of the resonances were strongly affected by the addition of 5-doxylstearic acid, with the residues of the termini illustrating a slightly greater reduction in signal intensity. These results indicate that most of the amino acids are close to the zwitterionic lipid surface, with the hydrophobic peptide termini more strongly associated with the lipid micelle. For the central helix L^{256}–I^{267}, we do not observe a periodicity of the reduction in signal intensity, which would be expected for a helix lying on the lipid surface. The lack of the periodicity, previously observed for other peptides (*35*), was attributed to rapid averaging caused by the high temperature

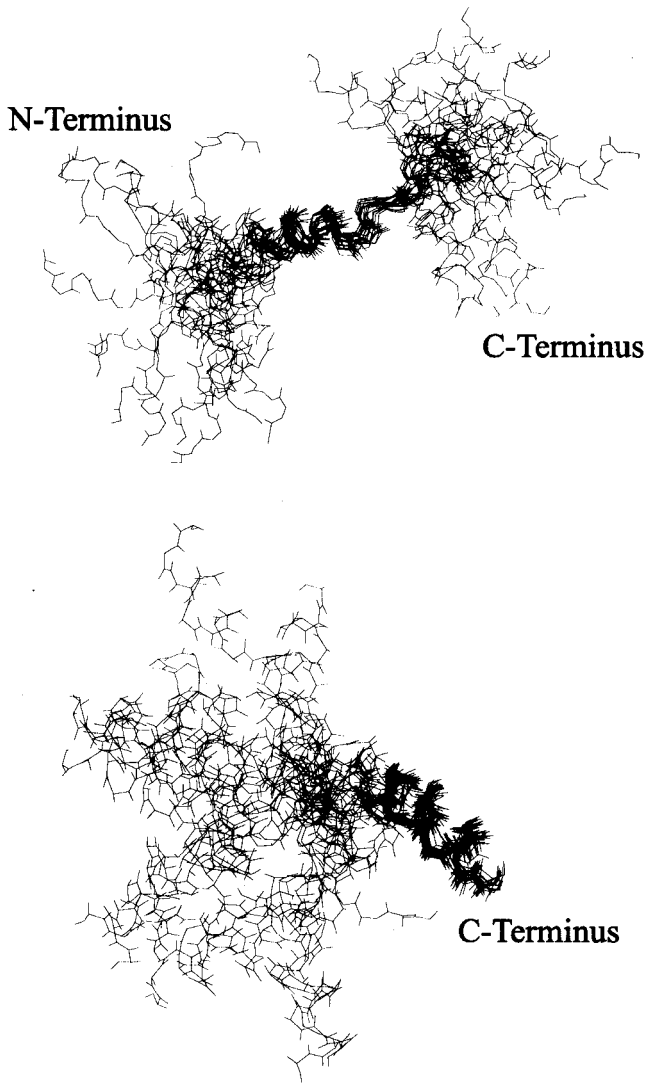

FIGURE 4: Superposition of 20 structures obtained from DG calculations. Heavy backbone atoms of residues 257–270 (top) and 274–285 (bottom) were used in the superposition.

(45 °C) necessary to maintain resolution of the proton signals. Because of the short length of the C-terminal helix (10 Å), which does not allow a greater insertion into the micelle, the 12-doxylstearic acid did not significantly affect residues in this region.

Molecular Dynamics. A low-energy DG conformation was chosen as a starting structure for the MD simulation. It was oriented in the biphasic water/decane cell with the central hydrophilic helix lying on the water–decane interface, with all of the charged residues projecting toward the solvent. The lipophilic residues of the two terminal tails were embedded into the decane phase. In particular, the C-terminal helix was pointing toward the core of the micelle.

During the simulation, the dihedral angles of the residues E^{252}–Q^{266} and A^{275}–A^{284} converge toward standard α-helical values while the N-terminus, D^{241}–G^{247}, adopted different extended conformations. In general, the secondary structure elements of the receptor fragment did not show significant changes during the MD simulation, with the exception of adopting more standard α-helix values for the central helix.

In contrast to the preservation of the secondary structure, there are changes in the tertiary structure during the MD

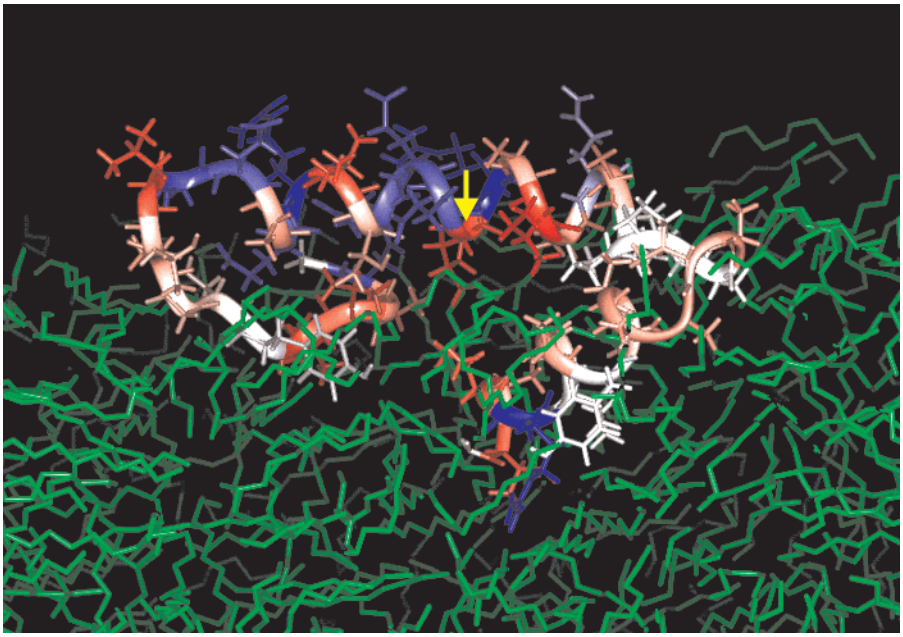

FIGURE 5: Structure of PTH1R(241−285) from the MD simulation in the water/decane simulation cell. The peptide residues are colored according to side chains hydrophobicity (blue polar, red hydrophobic). Decane molecules are depicted in green; the water molecules are not displayed for clarity. Residues belonging to TM2 and TM3 are embedded into decane phase. The yellow arrow indicates the location of L^{261}.

simulation. Both of the termini bend inwardly toward the decane−water interface and embed further into the decane layer, reducing their relative distance from 50 Å (in the DG-generated structure) to approximately 20 Å. The central helix is found in the water phase just above the interfacial surface, with most of the hydrophobic residues projecting toward the lipophilic (decane) surface (see Figure 5).

DISCUSSION

The standard development of models for G-protein-coupled receptors requires a definition of the TM helices, which is based on the recognition of characteristically hydrophobic sequences. However, with the discontinuity of physical properties at the lipid−water interface and the presence of stable secondary structure elements in the extracellular region, the accurate identification of the boundaries of the TM helices can be very difficult.

Spectroscopic studies of PTH in micellar systems clearly indicate a strong association with the lipid environment (*60*). Coupled with the data from cross-linking studies, implicating the location of residues participating in contact interactions with PTH to be at the extracellular membrane surface of PTH1R (*39*−*42*), the errors in the definition of the boundaries of the TM helices can have dramatic consequences on the capability of these receptor models to properly describe ligand binding and signaling processes. With this in mind, we have undertaken the experimental examination of the extracellular regions of PTH1R (*35*). The results from these studies provide the structural preferences of the extracellular regions of PTH1R that can then be incorporated into the receptor models. Here, the results from the examination of the first ECL, PTH1R(241−285), in the presence of DPC micelles are presented.

All of the NMR data (chemical shift indices, DG calculations, and NOE-restrained MD simulations) indicate a well-defined, hydrophobic helix spanning residues A^{275}−A^{284}. This helix contains approximately three α-helical loops that, according to nitroxide radical titration and MD simulations, are embedded into the micellar environment. These results characterize the beginning of TM3, which is one helical-turn longer than that predicted from homology modeling and hydropathicity plots (*16*). This additional helical turn places C^{281} (replaced with norleucine for this investigation) within TM3. This cysteine residue is implicated in the formation of a disulfide bond with C^{351} in the center of the second ECL. To form this disulfide bond, the small ECL2 must fold over in proximity to TM3.

The N-terminus of PTH1R(241−285) exhibits a long loop embedded into the membrane, with no stable secondary structure elements detected. Only the Hα secondary shifts and some short-range NOE interactions [$d_{N,N}(i, i + 1)$ $d_{\alpha N}(i, i + 2)$, see Table 1] suggest the presence of a folded conformation involving residues D^{241}−L^{244}. We propose that these residues constitute the C-terminal end of TM2. Unfortunately, we did not include in the synthetic peptide a sufficient number of residues from TM2 to create a long-lasting, stable, better anchored hydrophobic helix. Therefore, the experimental data do not allow for the determination of the relative topological arrangement of the peptide termini. The results from the NOE-restrained MD simulation suggest a global orientation with both termini projecting into the lipid environment, separated by a distance close to the value predicted for two adjacent helices in the rhodopsin-based receptor model (*18*, *19*).

Concerning the loop portion of PTH1R(241−285), we observe a well-defined α-helix between residues L^{256}−I^{264}, containing many charged residues that are largely exposed to the solvent. During the MD simulations, this motif extends toward A^{253} and A^{267}, but more realistically, the DG structures suggest less order, with 3^{10}-like loops at the extremities of the central helical fragment, in agreement with the $d_{\alpha N}(i, i + 2)$ interactions and lower values of the

Table 1: Average Dihedral Angles and Standard Deviation from the NOE-restrained MD Simulation of PTH1R(241−285) in a Decane/Water Simulation Cell

	ϕ	ψ
D^{241}	−84.5 ± 33.3	−77.6 ± 24.6
A^{242}	−85.1 ± 17.8	−3.9 ± 39.9
V^{243}	−98.1 ± 20.2	19.3 ± 62.2
L^{244}	−99.4 ± 15.3	69.7 ± 14.2
Y^{245}	−83.0 ± 30.9	−64.0 ± 41.6
S^{246}	49.2 ± 14.2	−48.9 ± 124.6
G^{247}	31.7 ± 40.6	−8.8 ± 34.4
A^{248}	49.0 ± 17.0	55.0 ± 17.6
T^{249}	−72.1 ± 14.3	−68.7 ± 14.6
L^{250}	−110.4 ± 16.8	−13.9 ± 20.7
D^{251}	59.9 ± 16.3	50.9 ± 25.0
E^{252}	−119.6 ± 18.4	−46.6 ± 8.3
A^{253}	−48.8 ± 11.8	−39.6 ± 16.1
E^{254}	−94.3 ± 10.6	−33.2 ± 8.0
R^{255}	−66.4 ± 8.0	−31.8 ± 7.6
L^{256}	−69.6 ± 9.5	−37.3 ± 13.0
T^{257}	−72.9 ± 13.7	−31.8 ± 8.2
E^{258}	−56.9 ± 7.3	−50.5 ± 7.2
E^{259}	−64.7 ± 9.5	−24.9 ± 20.2
E^{260}	−73.4 ± 20.5	−58.8 ± 12.3
L^{261}	−78.6 ± 16.4	−34.5 ± 13.6
R^{262}	−62.5 ± 10.1	−39.3 ± 8.2
A^{263}	−58.5 ± 9.2	−41.1 ± 13.7
I^{264}	−72.1 ± 10.7	−43.8 ± 8.1
A^{265}	−58.7 ± 10.2	−17.1 ± 21.5
Q^{266}	−97.1 ± 22.4	−37.9 ± 16.8
A^{267}	−45.4 ± 30.8	100.4 ± 14.8
P^{268}	−57.1 ± 13.3	134.8 ± 17.2
P^{269}	−47.2 ± 15.9	131.6 ± 13.0
P^{270}	−50.5 ± 18.1	133.5 ± 14.4
P^{271}	−51.9 ± 15.8	−28.2 ± 13.9
A^{272}	−52.3 ± 11.3	−20.9 ± 15.2
T^{273}	−77.6 ± 17.2	−39.9 ± 12.7
A^{274}	76.6 ± 14.7	−52.3 ± 12.1
A^{275}	−67.7 ± 10.2	−43.7 ± 8.3
A^{276}	−68.3 ± 7.6	−33.9 ± 7.6
G^{277}	−57.3 ± 8.4	−54.5 ± 9.2
Y^{278}	−49.5 ± 8.3	−53.3 ± 6.6
A^{279}	−60.2 ± 7.1	−45.5 ± 9.9
G^{280}	−63.4 ± 13.5	−55.6 ± 14.7
B^{281}	−66.1 ± 7.15	−34.0 ± 6.6
R^{282}	−75.5 ± 11.7	−7.7 ± 14.1
V^{283}	−94.3 ± 9.1	−36.8 ± 7.4
A^{284}	−57.5 ± 8.8	−40.8 ± 16.6
V^{285}	−113.2 ± 15.0	71.0 ± 10.9

chemical-shift indices. Furthermore, the presence of the helix-breaking sequence, $P^{258}-P-P-P^{261}$, certainly contributes to the termination of this helix. Although this helix cannot be considered amphipathic, because of the prevalence and clustering of charged side chains, all of the hydrophobic residues of the helix are projecting toward the lipid surface.

In the preceding paper in this issue, the identification of a contact point between L^{261} of PTH1R and Lys^{27} of PTH, as part of a photoaffinity scanning of the receptor−hormone interface, was described (*43*). Residue L^{261} is located in the middle of the well-defined central helix pointing its side chain toward the membrane-like environment. Because of the high affinity of the hydrophobic Bpa moiety for lipophilic surroundings, the identification of hydrophobic (or hydrophobic-seeking amino acids) contact points from cross-linking experiments is anticipated. In fact, all of the cross-linking points detected with this technique seem to involve residues close to the lipid−aqueous phase interface (*39*−*42*). One would expect that replacement of L^{261} with an alanine (L261A) would weaken the anchoring of the central helix to the membrane surface, which may be one reason for the observed lack of cross-linking with the mutant (L261A)PTH1R. Since the mutated receptor displays affinity for PTH and efficacy similar to the wild-type receptor, the point mutation probably does not result in major topological changes at the bimolecular interface (*43*). Therefore, the reduced ability of the methyl of alanine (vs the methine of leucine) to stabilize the free radical produced during cross-linking may better account for the lack of photoinsertion into the mutant receptor. In the wild-type receptor, the counterpart for the positively charged Lys^{27} side chain of PTH is not L^{261} but the negative charges of the contiguous residues $E^{258}-E-E^{260}$ of PTH1R.

The structure of PTH(1−34) in a micellar environment includes two well-defined helical domains (3−10 and 21−32) (*60*). The long, amphipathic C-terminal helix, including residue Lys^{27}, was found to lie upon the surface of the zwitterionic lipid with the hydrophobic face projecting into the micellar environment. Both the $L^{256}-I^{264}$ helix of PTH1R and the C-terminal helix in PTH contain many charged residues, which could produce numerous intermolecular Coulumbic interactions. For example, one helical turn removed from Lys^{26} in both directions, negatively charged residues are found (Asp^{30} and Glu^{22}). Corresponding to these negatively charged residues, one helical turn removed from E^{259}, one finds two complementary positively charged residues (R^{255} and R^{262}) on PTH1R. Moreover, two positively charged residues (Arg^{25} and Lys^{27}) flank Lys^{26}, which juxtapose three negatively charged residues in the PTH1R, $E^{258}-E-E^{260}$.

Previously, we proposed that the C-terminal helix of PTH and the helical domain of the proximal N-terminus of PTH1R(180−189) contribute to ligand binding by interacting in an antiparallel arrangement (*16*, *35*, *40*). Although numerous Coulombic interactions between these two helical domains were examined, the energies detected were not sufficient to account for the binding affinity nor the ligand specificity displayed by the receptor (*16*). In fact, we could not distinguish between two alternative topologies of ligand binding (regarding the orientation of the C-terminal helix of PTH with respect to the receptor). It is clear that other regions of PTH1R are contributing to ligand binding. Indeed recent cross-linking results have shown a contact point between T^{33}/Q^{37} with Trp^{23} of PTHrP (*41*), clearly showing that the large, extracellular N-terminal domain of PTH1R is involved in ligand binding (*28*). The results presented here and in the accompanying paper show that ECL1 is also playing a role in hormone binding, possibly through Columbic helix−helix interactions. It is interesting to note that with the helical arrangement of the C-terminus of PTH, both Trp^{23} and Lys^{27} would project out in approximately the same direction. On the basis of these findings, we now propose the ligand−receptor binding mode depicted in Figure 6. Of the two previously published modes (*16*), this one is consistent with the combined cross-linking data and the experimental structural features of the ligand and receptor fragments.

We have presented the results of our spectroscopic investigations of PTH1R(241−285) in a membrane-mimetic environment. The linear peptide did not completely mimic the features of ECL1 within the receptor, with TM2 being too short to serve as a helical membrane-tethering point. Nevertheless, we were able to determine the presence of

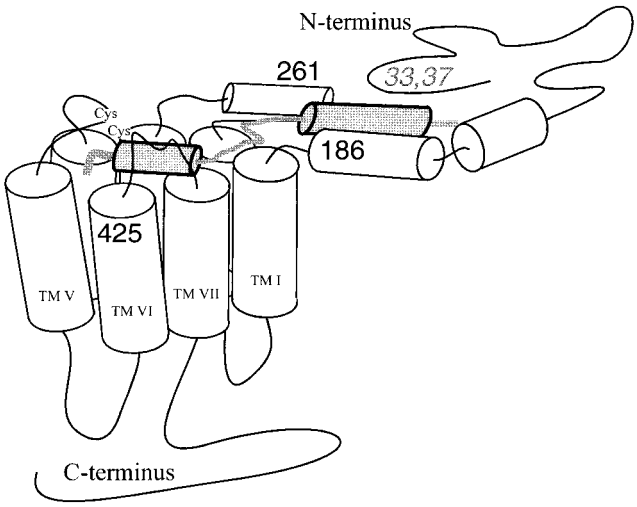

FIGURE 6: Schematic representation of the binding of PTH (shaded) to its G-protein-coupled receptor, PTH1R. The location of the contact points in PTH1R identified by photoaffinity cross-linking for PTH ($Ser^{1}-M^{425}$, $Lys^{13}-R^{186}$, $Lys^{27}-L^{261}$) and PTHrP ($Trp^{23}-T^{33}/Q^{37}$) are indicated. Structural features of the PTH and fragments of PTH1R are indicated in the figure.

important secondary structural elements. Three helical turns of TM3 were characterized, and the putative location of the C-terminal end of TM2 was determined; both are slightly different from the TM sequences predicted by homology modeling. A long hydrophilic helix in the middle of ECL1 was, for the first time, structurally characterized, and its topological orientation with respect to the micelle was determined using nitroxide radical titration and extensive MD simulations. These results provide unique insight into the bimolecular contact sites obtained from photoaffinity cross-linking experiments: on the basis of the structural features of ECL1, specific interresidue interactions within the ligand−receptor complex can be proposed, and insight into the topological arrangement of the ligand within the receptor can be generated.

ACKNOWLEDGMENT

We thank Maria Pellegrini (BASF, Worcester) for advice and assistance with the research described here and Chris Turner (MIT) for assistance with the 750-MHz instrument (supported through Grant RR-00995).

REFERENCES

1. Thorens, B. (1992) *Proc. Natl. Acad. Sci. U.S.A. 89*, 8641−8645.
2. Segre, G. V., and Goldring, S. R. (1993) *Trends Endocrinol. Metab. 4*, 309−314.
3. Jelinek, L. J., Lok, S., Rosenberg, G. B., Smith, R. A., Grant, F. J., Biggs, S., Bensch, P. A., Kuijper, J. L., Sheppard, P. O., Sprecher, C. A., et al. (1993) *Science 259*, 1614−1616.
4. Rosenblatt, M. (1981) *Pathobiol. Annu. 11*, 53−86.
5. Potts, J. T., Jr., Kronenberg, H. M., and Rosenblatt, M. (1982) *Adv. Protein Chem. 35*, 323−396.
6. Chorev, M., and Rosenblatt, M. (1994) in *The Parathyroids* (Bilezikian, J. P., Levine, M. A., Marcus, R., Eds.) pp 139−156, Raven Press, New York.
7. Mierke, D., and Pellegrini, M. (1999) *Curr. Pharm. Des. 5*, 21−36.
8. Mannstadt, M., Juppner, H., and Gardella, T. J. (1999) *Am. J. Physiol. 277*, F665−F675.
9. Raisz, L. G. (1999) *J. Bone Miner. Metab. 17*, 79−89.
10. Suva, L. J., Winslow, G. A., Wettenhall, R. E., Hammonds, R. G., Moseley, J. M., Diefenbach-Jagger, H., Rodda, C. P., Kemp, B. E., Rodriguez, H., Chen, E. Y., et al. (1987) *Science 237*, 893−896.
11. Fenton, A. J., Kemp, B. E., Kent, G. N., Moseley, J. M., Zheng, M. H., Rowe, D. J., Britto, J. M., Martin, T. J., and Nicholson, G. C. (1991) *Endocrinology 129*, 1762−1768.
12. Abou-Samra, A. B., Uneno, S., Jueppner, H., Keutmann, H., Potts, J. T., Jr., Segre, G. V., and Nussbaum, S. R. (1989) *Endocrinology 125*, 2215−2217.
13. Orloff, J. J., Wu, T. L., Heath, H. W., Brady, T. G., Brines, M. L., and Stewart, A. F. (1989) *J. Biol. Chem. 264*, 6097−6103.
14. Nissenson, R. A., Diep, D., and Strewler, G. J. (1988) *J. Biol. Chem. 263*, 12866−12871.
15. Juppner, H., Abou-Samra, A. B., Uneno, S., Gu, W. X., Potts, J. T., Jr., and Segre, G. V. (1988) *J. Biol. Chem. 263*, 8557−8560.
16. Roelz, C., Pellegrini, M., and Mierke, D. F. (1999) *Biochemistry 38*, 6397−6405.
17. Horn, F., Bywater, R., Krause, G., Kuipers, W., Oliveira, L., Paiva, A. C., Sander, C., and Vriend, G. (1998) *Recept. Channels 5*, 305−314.
18. Unger, V. M., Hargrave, P. A., Baldwin, J. M., and Schertler, G. F. (1997) *Nature 389*, 203−206.
19. Baldwin, J. M., Schertler, G. F., and Unger, V. M. (1997) *J. Mol. Biol. 272*, 144−164.
20. Pebay Peyroula, E., Rummel, G., Rosenbusch, J. P., and Landau, E. M. (1997) *Science 277*, 1676−1681.
21. Henderson, R., Baldwin, J. M., Ceska, T. A., Zemlin, F., Beckmann, E., and Downing, K. H. (1990) *J. Mol. Biol. 213*, 899−929.
22. Lee, C., Luck, M. D., Juppner, H., Potts, J. T., Jr., Kronenberg, H. M., and Gardella, T. J. (1995) *Mol. Endocrinol. 9*, 1269−1278.
23. Gardella, T. J., Luck, M. D., Fan, M. H., and Lee, C. (1996) *J. Biol. Chem. 271*, 12820−12825.
24. Bergwitz, C., Jusseaume, S. A., Luck, M. D., Juppner, H., and Gardella, T. J. (1997) *J. Biol. Chem. 272*, 28861−28868.
25. Carter, P. H., Shimizu, M., Luck, M. D., and Gardella, T. J. (1999) *J. Biol. Chem. 274*, 31955−31960.
26. Sheikh, S. P., Vilardarga, J. P., Baranski, T. J., Lichtarge, O., Iiri, T., Meng, E. C., Nissenson, R. A., and Bourne, H. R. (1999) *J. Biol. Chem. 274*, 17033−17041.
27. Jüppner, H., Schipani, E., Bringhurst, F. R., McClure, I., Keutmann, H. T., Potts, J. T., Jr., Kronenberg, H. M., Abou-Samra, A. B., Segre, G. V., and Gardella, T. J. (1994) *Endocrinology 134*, 879−884.
28. Lee, C., Gardella, T. J., Abou-Samra, A. B., Nussbaum, S. R., Segre, G. V., Potts, J. T., Jr., Kronenberg, H. M., and Jüppner, H. (1994) *Endocrinology 135*, 1488−1495.
29. Adams, A. E., Bisello, A., Chorev, M., Rosenblatt, M., and Suva, L. J. (1998) *Mol. Endocrinol. 12*, 1673−1683.
30. Huang, Z., Chen, Y., Pratt, S., Chen, T. H., Bambino, T., Nissenson, R. A., and Shoback, D. M. (1996) *J. Biol. Chem. 271*, 33382−33389.
31. Komatsu, Y., and Segre, G. V. (1998) in *American Society for Bone and Mineral Research* p S253, Elsevier, San Francisco.
32. Ferrari, S. L., Behar, V., Chorev, M., Rosenblatt, M., and Bisello, A. (1999) *J. Biol. Chem. 274*, 29968−29975.
33. Mierke, D. F., Royo, M., Pellegrini, M., Sun, H., and Chorev, M. (1996) *J. Am. Chem. Soc. 118*, 8998−9004.
34. Pellegrini, M., Royo, M., Chorev, M., and Mierke, D. F. (1996) *J. Pept. Sci. 40*, 653−666.
35. Pellegrini, M., Bisello, A., Rosenblatt, M., Chorev, M., and Mierke, D. F. (1998) *Biochemistry 37*, 12737−12743.
36. Pellegrini, M., and Mierke, D. F. (1999) *J. Peptide Sci. 51*, 208−220.
37. Yeagle, P. L., Alderfer, J. L., and Albert, A. D. (1997) *Biochemistry 36*, 9649−9654.
38. Yeagle, P. L., and Albert, A. D. (1998) *Biochem. Soc. Trans. 26*, 520−531.

39. Zhou, A. T., Bessalle, R., Bisello, A., Nakamoto, C., Rosenblatt, M., Suva, L. J., and Chorev, M. (1997) *Proc. Natl. Acad. Sci. U.S.A. 94*, 3644−3649.
40. Bisello, A., Adams, A. E., Mierke, D. F., Pellegrini, M., Rosenblatt, M., Suva, L. J., and Chorev, M. (1998) *J. Biol. Chem. 273*, 22498−22505.
41. Mannstadt, M., Luck, M. D., Gardella, T. J., and Juppner, H. (1998) *J. Biol. Chem. 273*, 16890−16896.
42. Behar, V., Bisello, A., Rosenblatt, M., and Chorev, M. (1998) in *ASBMR-IBMS, 2nd Joint Meeting*, pp SA-176, Elsevier, San Francisco.
43. Greenberg, Z., Bisello, A., Mierke, D. F., Rosenblatt, M., and Chorev, M. (2000) *Biochemistry 39*, 8142−8152.
44. Nakamoto, C., Behar, V., Chin, K. R., Adams, A. E., Suva, L. J., Rosenblatt, M., and Chorev, M. (1995) *Biochemistry 34*, 10546−10552.
45. Delaglio, F., Grzesiek, S., Vuister, G. W., Zhu, G., Pfeifer, J., and Bax, A. (1995) *J. Biomol. NMR 6*, 277−293.
46. Piotto, M., Saudek, V., and Sklenar, V. (1992) *J. Biomol. NMR 2*, 661−665.
47. Wishart, D. S., Sykes, B. D., and Richards, F. M. (1992) *Biochemistry 31*, 1647−1651.
48. Brown, L. R., Bösch, C., and Wüthrich, K. (1981) *Biochim. Biophys. Acta 642*, 296−312.
49. Papavoine, C. H. M., Konings, R. N. H., Hilbers, C. W., and van de Ven, F. J. M. (1994) *Biochemistry 33*, 12990−12997.
50. Wuthrich, K. (1986) *NMR of Proteins and Nucleic Acids*, John Wiley, New York.
51. Crippen, G. M., and Havel, T. F. (1988) *Distance Geometry and Molecular Conformation*, John Wiley, New York.
52. Havel, T. F. (1991) *Prog. Biophys. Mol. Biol. 56*, 43−78.
53. Mierke, D. F., Geyer, A., and Kessler, H. (1994) *Int. J. Pept. Protein Res. 44*, 325−331.
54. Mierke, D. F., Scheek, R. M., and Kessler, H. (1994) *Biopolymers 34*, 559−563.
55. Berendsen, H. J. C., van der Spoel, D., and van Buuren, R. (1995) *Comput. Phys. Commun. 95*, 43−56.
56. van Buuren, A. R., Marrink, S., and Berendsen, H. J. C. (1993) *J. Phys. Chem. 97*, 9206−9216.
57. Pellegrini, M., and Mierke, D. F. (1999) *Biochemistry 38*, 14775−14783.
58. Opella, S. J., Marassi, F. M., Gesell, J. J., Valente, A. P., Kim, Y., Oblatt-Montal, M., and Montal, M. (1999) *Nat. Struct. Biol. 6*, 374−379.
59. Havel, T. F. (1990) *Biopolymers 29*, 1565−1585.
60. Pellegrini, M., Royo, M., Rosenblatt, M., Chorev, M., and Mierke, D. F. (1998) *J. Biol. Chem. 273*, 10420−10427.

BI000196F